Sensors and Actuators B 194 (2014) 10–18

Contents lists available at ScienceDirect

Sensors and Actuators B: Chemical

journal homepage: www.elsevier.com/locate/snb

Label-free detection of DNA hybridization using nanopillar arrays based optical biosensor

Jem-Kun Chen [a,*], Gang-Yan Zhou [a], Chi-Jung Chang [b], Chih-Chia Cheng [c]

[a] Department of Materials Science and Engineering, National Taiwan University of Science and Technology, 43, Sec. 4, Keelung Road, Taipei 106, Taiwan, ROC
[b] Department of Chemical Engineering, Feng Chia University, 100, Wenhwa Road, Seatwen, Taichung 40724, Taiwan, ROC
[c] Department of Applied Chemistry, National Chiao-Tung University, Hsinchu 300, Taiwan, ROC

ARTICLE INFO

Article history:
Received 19 August 2013
Accepted 19 December 2013
Available online 27 December 2013

Keywords:
Two-dimensional periodic grating
Refractive index
Effective medium theory
DNA hybridization
Nanopillar array

ABSTRACT

In this study we fabricated nanopillar arrays (NPLAs) of silicon, through a process involving very-large-scale integration and reactive ion etching, for use as two-dimensional periodic relief gratings on silicon surfaces. Oligonucleotides were successively immobilized on the pillar surface, allowing the system to be used as an optical detector specific for the targeted single-stranded DNAs (ssDNAs). The surfaces of the oligonucleotides-modified NPLAs underwent insignificant structural changes, but upon hybridizing with target ssDNA, the NPLAs underwent dramatic changes in terms of their pillar scale. Binding of the oligonucleotides to the NPLA occurred in a way that allowed them to retain their function and selectively bind the target ssDNA. We evaluated the performance of the sensor by capturing the target ssDNA on the NPLA and measuring the effective refractive index (n_{eff}). The binding of the target ssDNA species to the NPLA resulted in a color change from pure blue to red, observable by the naked eye at an angle of 15°. Moreover, we used effective medium theory to calculate the filling factors inside the NPLA and, thereby, examine the values of n_{eff} during the structural changes of the NPLA. Accordingly, these new films have potential applications as label-free optical biosensors.

1. Introduction

Recent advances and demands in the field of molecular diagnostics, molecular medicine, and forensics have propelled the development of highly selective and sensitive nucleotide sensors. Reduced sample volumes and low analyte concentrations have presented a challenge to the current detection technology. DNA hybridization-based detection is a major technique for the diagnosis of genetic disease, where clinical symptoms are linked to DNA alterations [1]. DNA hybridization is highly specific and becomes very sensitive when coupled with an optical detection scheme. Optical detection schemes usually require some kind of labeling such as the use of molecular beacons [2] or fluorophore tagging [3]. Typically, organic fluorophores and quantum dots are used for signaling the detection of the hybridization of DNA [4]. These fluorophores are usually excited at shorter wavelengths and emit at longer wavelengths. The labeling process could sometimes become very challenging, costly, and time-consuming, and may lead to occlusion of hybridization sites due to steric hindrance. Thus, label-free detection schemes would bring about the obvious benefits of being simple, quick, easy, and cost-effective [5]. There have been a number of label-free optical detections reported in the literature, such as well-known surface plasmon resonance (SPR), and conjugated polymers amplification with the use of intercalating dye, among others [6].

Among the many available biosensing platforms, optical diffraction-based biosensors are effective for recognizing the binding events of various biomolecules; these systems operate based on changes in effective height or refractive index on periodically patterned gratings [7,8]. Recently, several different types of optical biological sensors have been reported that function through the measurement of diffraction patterns as the assay readout; alternatively, these optical detection methods could employ surface plasmon resonance (SPR) [9], ordered structures [10], surface acoustic waves [11], and fiber optical techniques [12]. The sensor described in that earlier paper, however, the reproducibility of the inactivation of the scale-up of fabrication would be problematic when using that approach. Moreover, the change in refractive index across the interface as a result of protein adsorption was small. Although optical reflectometry, SPR, and ellipsometry base their measurements on detecting changes in refractive index and they can provide useful estimates of degrees of adsorption, they have little inherent sensitivity to the layer thickness or composition [13,14]. In many studies, the detection of small amounts of

* Corresponding author. Tel.: +886 2 27376523; fax: +886 2 27376544.
E-mail address: jkchen@mail.ntust.edu.tw (J.-K. Chen).

0925-4005/$ – see front matter © 2013 Elsevier B.V. All rights reserved.
http://dx.doi.org/10.1016/j.snb.2013.12.071

biomolecules require additional signal enhancement [15], which can be accomplished through either microfabrication of solid diffraction gratings or self-fabrication of in situ-assembled diffraction gratings from nano- or micro-size particles [16].

Nanopillar array (NPLA) surfaces are attractive components of new optical elements; indeed, many different elements presenting such surfaces have been developed previously. Through careful design of the NPLA structure, highly efficient diffraction gratings can be synthesized, even with a binary profile. When the NPLA element is a one-dimensional (1D) periodic surface or an unsymmetrical two-dimensional (2D) periodic surface, the effective refractive index depends upon the polarization states of the incident light (Fig. 1) [17,18]. Symmetrical 2D periodic surfaces are currently attracting great interest for their potential applications in gratings or photonics [19]. The 1D geometries of NPLAs can result in unique optical properties, including polarized photoresponses, and biosensing [20]. When the NPLAs interact specifically or nonspecifically with target molecules, changes typically occur to the geometrical parameters of the gratings and/or the refractive index contrast [21]. These materials have been exploited extensively in various technological applications ranging from sensitive chemical and biological sensing and nano-optical devices to magnetic memories and logic circuits [22]. Many top-down and bottom-up technologies have been developed for the fabrication of functional NPLAs [23,24]. Very-large-scale integration (VLSI) is currently a popular top-down technique for fabricating nanopillars possessing arbitrary structures [25]. Because the appearance of 1D periodic relief gratings (1DPRGs) can be quite sensitive to the observation angles α and β (Fig. 1) under transverse magnetic (TM) and transverse electric (TE) polarization, they always display composed color images [7,10,26]. Unlike 1DPRGs, the color of an NPLA, as observed by the naked eye, is dependent solely on the angle β, thereby providing improved stability and chromatic aberration without restricting the visual angles. The immobilization of oligonucleotides onto the surface of NPLAs and the subsequent capture of target single-stranded DNAs (ssDNAs) from sample solutions can change the geometrical parameters and refractive indices of the gratings [27]. In this present study, we used VLSI techniques to generate NPLAs of silica for use as 2D periodic relief gratings, thereby increasing the interface arising from biomacromoles and to enhancing the optical sensitivity. The detection of the oligonucleotides bound to the NPLA nanostructures has been achieved by illuminating the surface with visible light because the degree of diffraction is influenced by the binding of the biological material. Specifically, the target ssDNA-induced nanostructural variation in the NPLA system enables large-scale morphological reorganization, resulting in changes in the effective refractive index. This versatile process is particularly amenable to the creation of large-area uniform coatings on essentially any surface, with precise control over the pillar scale of silicon and the optical properties of the target ssDNA.

2. Experimental

2.1. Materials

Single-crystal Si wafers, Si(1 0 0), polished on one side (diameter: 6 inch) were supplied by Hitachi (Japan) and cut into 1.5 cm × 1.5 cm samples. To remove dust particles and organic contaminants, the Si surfaces were ultrasonically rinsed sequentially with methanol, acetone, and dichloromethane for 10 min each and subsequently dried under vacuum. The materials used for fabrication and characterization of the oligonucleotides modified NPLAs were purchased from Acros Organics and used without further purification. Fresh 3-(mercaptopropyl)trimethoxysilane (MPTES), purchased from Acros Organics, was used since it is subject to oxidation of the SH groups and crosslinking of the molecules due the hydrolysis of silanol groups when humidity condenses inside the bottle. Thiolated oligonucleotides were purchased from Synthetic Genetics (San Diego, CA). Two kinds of oligonucleotides that were immobilized onto the MPTES layer possessed the sequence 5′-HS-C_{18}-ATGACTAAGCTGTTACTACGG-3′ (FS) and 5′-HS-C_{18}-TTATTCAGCTCCAATTATTATAT-3′ (RS), forward and reverse complementary sequences of *S. aureus* panC gene (GenBank accession number YP_501370.1), respectively [28]. All other chemicals and solvents were of reagent grade and purchased from Aldrich Chemical.

2.2. Oligonucleotides immobilization on NPLA

The basic strategy for the fabrication of the oligonucleotides-modified NPLA using the VLSI process and reactive ion etching (RIE) is depicted in Fig. 2. (A) The Si wafer was treated with hexamethyldisilazane in a thermal evaporator (Track MK-8) at 90 °C for 30 s to transform the OH groups on the surface of wafer into an inert film of $Si(CH_3)_3$ groups for photoresist coating [29]. Negative photoresist was spun onto the HMDS-treated Si wafer; advanced lithography was then used to pattern the photoresist as an NPLA after development. (B) RIE (Plasma Etcher, TEL TE5000) was used for the dry etching process, with the photoresist NPLA on the silicon wafer employed as a protection mask. Only the exposed regions of silicon were dry-etched by supplying a gas mixture of CHF_3 and CF_4 under RIE processing conditions at an etching rate of 475.2 nm/min. (C) Subsequently, the remaining photoresist hard mask was removed from the surface through immersion in solvents, leaving behind an NPLA of silicon. (D) The silicon NPLAs were then immersed in the mixture of HNO_3 and H_2O_2 (2:1, mol%) for 10 min and subsequently rinsed with doubly distilled water a minimum of five times to oxidize the silicon NPLA [30]. (E) The NPLA of silicon oxide was immersed in a solution of MPTES (1.5 wt%) in toluene to assemble the thiol groups on the surface [31]. (F) Thiol-terminated oligonucleotide probes FS and RS were diluted in sodium chloride/sodium citrate (SSC) buffer (3 M NaCl, 0.3 M Na citrate–$2H_2O$, pH 4.5, Aldrich) to a final concentration of between 50 and 200 nM. The oligonucleotide buffered solution was dropped onto freshly MPTES-modified NPLAs using a pipette. These surfaces were subsequently incubated for 16 h at 20 °C in a humidified chamber (54% relative humidity) to prevent spot drying (which can lead to uneven distribution) and then washed three times with water and buffer solution. Finally, the surfaces were dried with nitrogen gas. Commercially available recombinant oligonucleotides were covalently immobilized on the MPTES-modified NPLA surface through disulfide bridges to give oligonucleotides-NPLAs. The sample was cleaned ultrasonically for 90 min to separate any unbounded oligonucleotide, placed in PBS, and then the cleaning process was repeated until no oligonucleotide was recovered in the supernatant. Finally, the resulting NPLA was kept wetted until required for further use, thereby yielding a promising general platform for the specific and sensitive detection of the target ssDNA in terms of the effective refractive index. Target ssDNA of *S. aureus* panC gene and fully immobilized surfaces of FS and RS were subsequently incubated for 6 h at 10 °C in a hybridization buffer solution (consisting of 1.8 M SSC pH 7, Denhardt's solution (1%, w/v BSA (bovine serum albumin), 2% Ficoll 400, and 2% polyvinylpyrrolidone (PVP)), 0.5% sodium dodecyl sulfate (SDS), and sheared salmon sperm DNA (55 μg/mL) to a final concentration of 400 nM). Control ssDNA of *E. coli* cells was also tested in the same condition to evaluate the selectivity of the oligonucleotides-NPLAs.

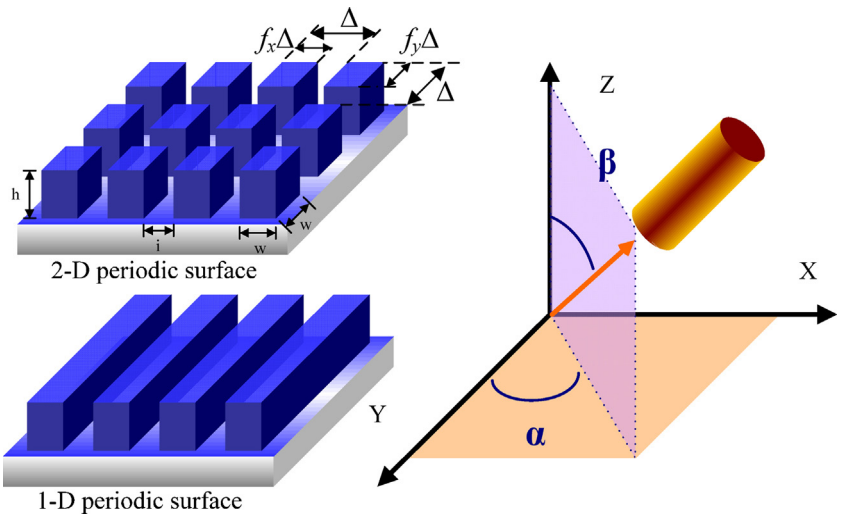

Fig. 1. Symmetric 1D and 2D periodic relief gratings with filling factor in the *x* and *y* directions. Schematic representation of the angles α and β, defined as the observation angles of a grating in the *x*–*y* plane and vertical to the *x*–*y* plane, respectively, of light reflected from an NPLA surface.

2.3. Characterization of oligonucleotides-modified NPLA through a ssDNA hybridization

XPS is a quantitative, surface analytical tool sensitive to the atomic composition of the outermost 100 Å of a sample surface. XPS measurements were performed on a Scientific Theta Probe (U.K.) instrument using a monochromatic Al KR X-ray source and a 75° take-off angle. The take-off angle is defined as the angle between the sample surface normal and the axis of the XPS analyzer lens. Compositional survey and detailed scans (Si 2p, C 1s, N 1s, O 1s and S 2p) were acquired using a pass energy of 80 eV. High-resolution spectra (Si 2p, C 1s, N 1s, O 1s and S 2p) were acquired for the NPLA samples using a pass energy of 20 eV. Three spots on two or more replicates of each sample were analyzed. Reported compositional data were averages of values determined at each spot.

All samples after immersion into the various phosphate buffer solutions for 10 min are lyophilized under −40 °C for 10 min to remove the solvent in vacuum freeze dryer (BENCHTOP 2K; VIRTIS; America). All measurements were performed on lyophilized samples in the air to obtain stable results. We used a spectroscopic ellipsometer with a beam diameter of 5 mm (SOPRA SE-5, France) to measure ellipsometric parameters, $\Psi(\lambda)$ and $\Delta(\lambda)$, of the NPLA films on silicon substrates at λ = 245–1000 nm at incidence angles of 75°. These measurements were carried out by recording $\Psi(\lambda)$ and $\Delta(\lambda)$ spectra after a certain time interval typically of 20–30 s in the course of phase transition of NPLA (where Ψ is the amplitude (A) ratio $\tan(\Psi) = A_p/A_s$ and Δ the phase shift $\Delta = \varphi_p - \varphi_s$ between p- and s-components of polarized light of wavelength λ). Because of possible interference due to changes of the refractive index of NPLAs during the course of the experiment, fitting was performed by selecting Ψ or/and Δ data points at a certain wavelength (λ) from a massive Ψ, Δ (λ, t) file. The shape (raising or decaying) of $\Psi(t)$ and $\Delta(t)$ curves depends on the wavelength selection on either the decreasing or rising part of $\Psi(\lambda)$, $\Delta(\lambda)$ spectra, respectively [32]. The details of ellipsometry data fitting are given in analysis software mounted on the ellipsometer. In addition, we used a single-wavelength ellipsometer (λ = 632.8 nm, He–Ne laser) with a beam diameter of 1 mm (DHA-OLX3, Mizojiri Optical) to deduce the variations of the refractive index and thickness in the measured areas for each NPLA film.

The morphologies of various patterns of NPLAs were analyzed using an atomic force microscope (AFM; Veeco Dimension 5000 scanning probe microscope). AFM images were recorded in a tapping mode under ambient conditions with a Multimode Nanoscope III scanning probe microscope from Digital Instruments. UV–vis–NIR reflected spectra were acquired using a Shimadzu 3600 UV–vis–NIR spectrophotometer.

2.4. Optical properties of the oligonucleotides-modified NPLA for ssDNA hybridization

To readily fabricate artificial dielectric elements, the effective index must be relatable to the grating profile in a simple manner. By solving Maxwell's equations with relevant boundary conditions, the effective indices of 1D and 2D subwavelength gratings have been obtained numerically by many authors [33]. Alternatively, the use of effective medium theory generally yields a good approximation if the period-to-wavelength ratio is sufficiently small. For 1D gratings, the theory provides the following simple expressions for the ordinary and extraordinary indices:

$$n_{TE}^2 = f_1 n_1^2 + f_2 n_2^2 \quad (1)$$

$$n_{TM}^{-2} = f_1 n_1^{-2} + f_2 n_2^{-2} \quad (2)$$

where f_1 is the fill factor for medium 1 and f_2 (equal to $1 - f_1$) is the fill factor for medium 2. In the case of a 1D binary relief grating, the effective refractive indices for TE and TM polarizations are n_{TE} and n_{TM}, respectively. The different indices for the two polarization states indicate that 1D subwavelength gratings exhibit form birefringence. For the convenience, the fill factors in the *x* directions is set to equal to that in *y* direction for description of the square pillar structure. The refractive index in the direction normal to the grating vectors of a 2D subwavelength grating is given in effective medium theory by

$$n_{eff} = [(1 - f^2)n_1^2 + f^2 n_2^2]^{1/2} \quad (3)$$

where f_x and f_y are the fill factors of medium 2 in the *x* and *y* directions, respectively (Fig. 1). It has been noted that there are no simple closed-form zero-order expressions for the transverse principal effective indices of a 2D subwavelength grating [34]. On the other hand, the indices can be bounded approximately by use of simple expressions derived from effective medium theory [35]. For simplicity, only square cylindrical geometries were considered in this study. To set the upper bound, the 2D rectangular grating

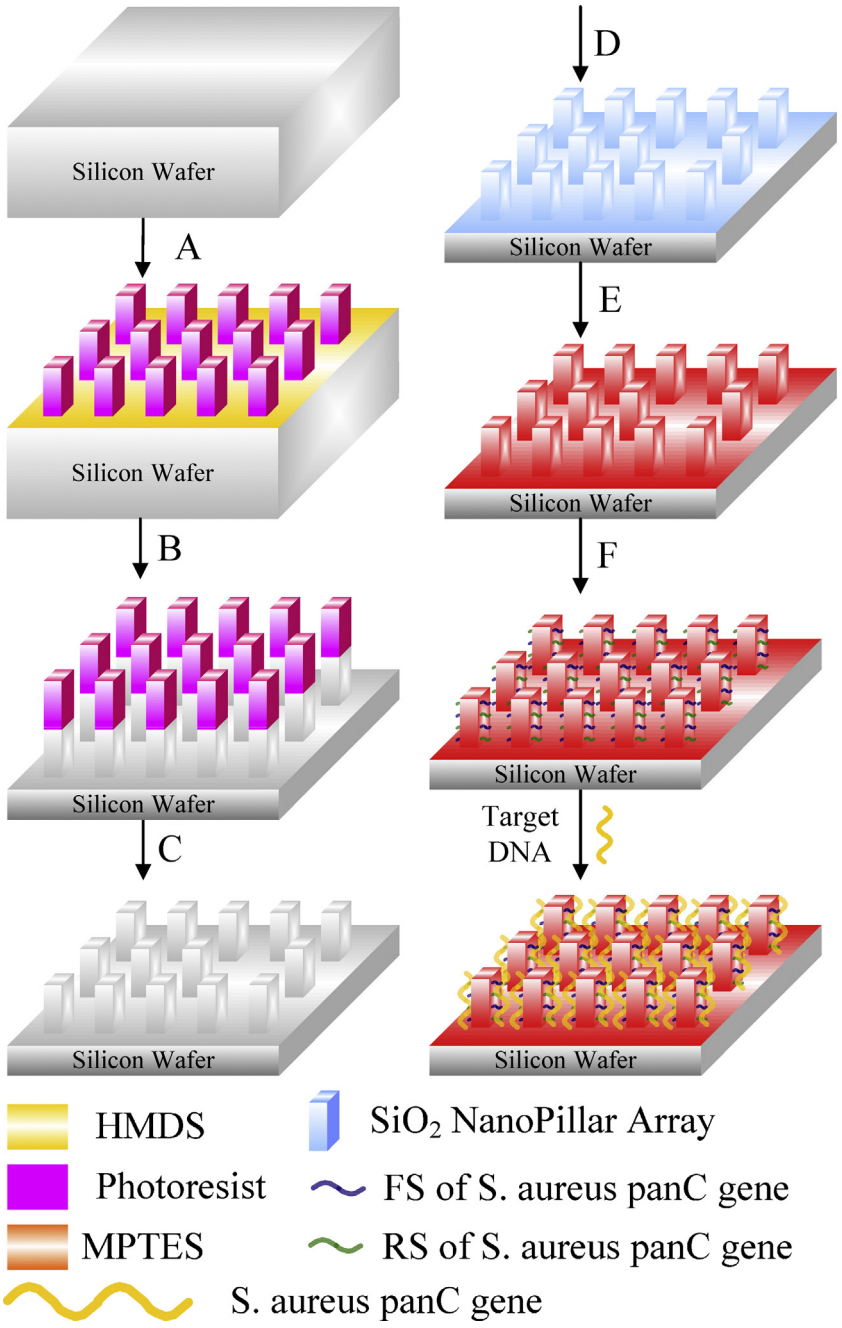

Fig. 2. Schematic representation of the process used to fabricate the oligonucleotides-modified NPLA. (A) Silicon wafer surface was treated with HMDS in a thermal evaporator. Negative photoresist was spun onto the HMDS-treated surface to pattern the photoresist as a NPLA. (B) Only the exposed regions of silicon dioxide were dry-etched by supplying a mixture gas of CHF_3 and CF_4. (C) The remaining photoresist hard mask was then removed from the surface through the action of solvents. (D) The silicon NPLAs were then treated with mixture of HNO_3 and H_2O_2 (2:1, mol%) to oxidize the silicon NPLA. (E) The NPLA of silicon oxide was treated with MPTES to assemble an array of thiol groups. (F) The NPLA presenting thiol groups was treated with a solution of FS and RS to immobilize oligonucleotides on the pillar surfaces to hybridize with target ssDNA; the presence of target ssDNA could be detected through ellipsometry because of the geometric change of NPLA.

was viewed as a 1D grating consisting of strips aligned perpendicular to the electric field. Each strip, in turn, could be considered a section of a 1D grating with ridges parallel to the electric field. The effective refractive index of each strip was calculated using Eq. (1). These strip indices were then used to calculate the overall effective refractive index, using Eq. (2). This effective index, an upper bound that is exact in the static case, is given by

$$n_{\text{eff,upper}} = \left[\frac{1-f}{n_1^2} + \frac{f}{fn_2^2 + (1-f)n_1^2}\right]^{-1/2} \quad (4)$$

To obtain the lower bound, the 2D grating was viewed as a 1D grating consisting of strips parallel to the electric field. The effective refractive index of each strip was found using Eq. (2) and the overall effective index, representing the lower bound, from Eq. (1), giving

$$n_{\text{eff,lower}} = \left[(1-f)n_1^2 + \frac{f}{fn_2^{-2} + (1-f)n_1^{-2}}\right]^{-1/2} \quad (5)$$

At all times, the bounds were positioned between the indices of the two components of the artificial dielectric.

3. Results and discussion

3.1. Surface concentrations of immobilized oligonucleotides and bound target ssDNA on NPLAs

XPS was used to obtain detailed information about the chemical composition of NPLA surfaces at various stages during the surface modification process. Two peak components at the binding energies (BE) of ca. 99 and 103 eV, attributable to Si—Si and Si—O species, respectively, appear in the Si 2p core-level spectrum of the pristine Si(1 0 0) surface. Oxidization of the silicon surface activated the surface with Si—O species, which enhanced a signal at a BE of 103 eV. C 1s core-level spectrum of the MPTES-functionalized silicon surface, curve-fitted with two peak components having BEs at ca. 283.9 and 284.6 eV, increased significantly because of the presence of C—H species of the MPTES layer on the surface [36]. In addition, the sulfur peak (S 2p) was detected at 163.7 eV, which indicated that all of the sulfur was present as thiol or disulfide. XPS was also used to study the composition of disulfide bridge after immobilization of oligonucleotides. The result indicates that S 2p region of a disulfide bridge formed on this silicon wafer. By subtracting the background, a S 2p doublet peak with binding energy at 163.8 and 165.1 eV can be resolved, corresponding to the embedded disulfide bond. It is very difficult to judge whether any of the disulfide bonds have been oxidized since the bulk plasmon band occurs in the same region as oxidized S 2p peaks [37]. Elements P and N are unique to DNA and are therefore good indicators of relative amounts of oligonucleotides and ssDNA present on the oligonucleotides-NPLA and ssDNA-oligonucleotides-NPLA surfaces at 134 and 399.5 eV, respectively. Table 1 summarizes the XPS elemental compositions from pristine silicon NPLA, silicon oxide NPLA, MPTES-NPLA, oligonucleotides-NPLA and ssDNA-oligonucleotides-NPLA. The values of the [C]/[S] ratio of the MPTES-NPLA surface obtained from XPS analysis was 4.5, respectively, which are in fairly good agreement with their theoretical ratio of 3, respectively. Fairly good agreements also exist between the XPS-derived and theoretical surface compositions of the oligonucleotides-NPLA (Table 1). In addition, the NPLA structure enhanced the hydrophobicity of the silicon surface. The silicon oxide NPLA exhibited the fully hydrophilic property. After the bonding of MPTES to the silicon surface, the contact angle increased from 0° to 68.5 ± 3°. The hydrophilicity of the oligonucleotides-NPLA facilitated the hybridizing with target ssDNA.

3.2. Morphological change of oligonucleotides-modified NPLA for selective ssDNA hybridization

When an oligonucleotides-modified NPLA couples specifically with its target ssDNA, change typically occur to the geometrical parameters of the NPLA and/or the refractive index contrast. According to the effective medium theory, the fill factors f_x and f_y represent the ratios of the pillar scale to the period in the x and y directions, respectively (Fig. 1). Fig. 3a presents 3D, 2D, and line cross-section analysis AFM topographic images of the oligonucleotides-modified NPLA, which existed on the Si surface as a dense distinctive overlayer, with pillar scales of approximately 176 nm, within a scanning area of 5 μm × 5 μm. The line cross-section analysis clearly reveals the pillar array texture. Each pillar of the oligonucleotides-modified NPLA had been fabricated successfully in a regular array and had a similar height of 361 ± 3 nm. The NPLA comprised a repeating pattern of pillars (176 ± 3 nm) and spaces (387 ± 3 nm) over a large area. We controlled the period of this grating so that it would be below the wavelength used to enhance the grating effect. The dimension of oligonucleotides is approximately 21 nm; their deposition increased the scale of the pillars, but decreased the space between them [38]. The oligonucleotides moieties bound to the pillar surface retained their ability to recognize and hybridize their partial complementary ssDNA efficiently and specifically. After the target ssDNAs had been given time to bind to the oligonucleotides, we washed the silicon surfaces in PBS solution; Fig. 3b presents 3D, 2D, and line cross-section analysis AFM topographic images of the oligonucleotides-modified NPLA after hybridizing to the target ssDNA. We observe that the regular pillar array remained after such processing. The scale of each pillar had increased from 176 ± 3 nm to 434 ± 3 nm, implying a decrease in the space between the pillars. The results suggest that the scale of the target ssDNA moiety is close to 129 ± 3 nm; such complexation might, therefore, change the scale of the pillars and the space between them. We suspect that other small DNAs (e.g., less than 100 base pairs) would probably not be detected with sufficient sensitivity when using this method. To verify that the target ssDNA moieties were bound only to the oligonucleotides-modified areas, we also bound control ssDNA of *E. coli* cells (dimensions: 143 ± 8 nm) to the surfaces as a control and then washed the silicon surfaces in PBS containing 0.5% Tween 20 (pH 7.4, 10 mM) at 10 °C (the inclusion of Tween in the buffer minimized nonspecific binding). We observed no apparent variation in the geometrical parameters over the entire sample area as a result of any specific binding, thereby confirming the functionality and specificity of the NPLAs. The degree of mismatch was negligible, as revealed by the control experiments. Despite the variations in their geometrical parameters, we conclude that these samples effectively bound target ssDNA, as measured in terms of the effective refractive index.

3.3. Effective refractive index for selective ssDNA hybridization

Through ellipsometry, we measured the refractive index of a thin film of MHHA at 632.8 nm, obtaining a value of 1.875 – close to that from a previous report [39] – for use as a standard. We further characterized of MHHA attached to the MAHA-modified NPLA in terms of the effective refractive index (n_{eff}) obtained using ellipsometry. Fig. 4a displays the values of n_{eff} of bare NPLA (A), MPTES-NPLA (B), and oligonucleotides-NPLA (C) obtained through environmental ellipsometry at a wavelength of 633 nm. The refractive index of target ssDNA is larger than that of silicon oxide (1.46); therefore, the average value (1.668) of refractive indices can be applied in effective medium theory. A dramatic response in the value of n_{eff}, as probed through ellipsometry, occurred specifically after hybridizing target ssDNA with oligonucleotides on the pillar surface [Fig. 4a(D)]. In addition, the value of n_{eff} of the oligonucleotides-modified NPLA remained relatively unchanged after treatment with the control ssDNA, confirming that control ssDNA did not bind significantly to the oligonucleotides moieties on the pillar surface [Fig. 4a(E)]. An NPLA can be regarded that an air layer filled by silicon oxide covered with target ssDNA; in Eq. (3), n_1 and n_2 represent the refractive indices of air and silicon oxide covered with target ssDNA, respectively. We calculated values of f by using our measured values of n_{eff}, calculated from the change in pillar scale after hybridizing with the target. The effective medium theory provides much more accurate results only when the period is sufficiently smaller than the wavelength of the incident light. Therefore, we use the bounded indices expressions to fit our results. The literature suggests that the effective indices are, on average, increased by at most 3% for a 2D 400-nm-period symmetric grating at a wavelength of 633 nm [34]. Therefore, we suspect the inaccuracy of our measurements of the refractive indices for the 176-nm-scale NPLA at a wavelength of 633 nm would be, on average, less than 3%. Fig. 4b presents the values of n_{eff} and f, modeled using Eqs. (4) and (5), of the bare NPLA (A), MPTES-NPLA (B), oligonucleotides-modified NPLA (C),

Table 1
XPS elemental compositional data for pristine silicon NPLA, silicon oxide NPLA, MPTES-NPLA, oligonucleotides-NPLA and ssDNA-oligonucleotides-NPLA.

Sample	Atomic percent[a]						Atomic ratio				Contact angle (°)
	Si 2p	C 1s	O 1s	N 1s	P 2p	S 2p	[C]/[S][b]	[O]/[S]	[N]/[S]	[P]/[S]	
Silicon NPLA	79.5	11.3	8.3	0.9	0.0	0.0	–	–	–	–	95.4 ± 3
Silicon oxide NPLA	54.2	5.1	40.4	0.3	0.0	0.0	–	–	–	–	0 ± 3
MPTES-NPLA	49.2	6.3	42.8	0.3	0.0	1.4	4.5 (3)[c]	30.6	–	–	68.5 ± 3
Oligonucleotides-NPLA	1.4	46.3	31.9	15.6	4.4	0.4	115.8 (110)	79.8 (84)	39.0 (38)	11.0 (12)	0 ± 3
ssDNA-oligonucleotides-NPLA	0.6	44.8	35.3	14.1	5.2	0.0	–	–	–	–	0 ± 3

[a] Determined from XPS core-level spectral area ratio. Values in parentheses are theoretical ratios.
[b] Determined from the XPS curve-fitted element core-level spectra.
[c] Values in parentheses are theoretical ratios.

oligonucleotides-modified NPLA after target ssDNA hybridizing (D), and oligonucleotides-modified NPLA after binding the control ssDNA (E), constructed to fit the data only at 633 nm to avoid the effects of the lower wavelengths of incident light that are absorbed strongly by the surface cover slip. The measured values of n_{eff} located within the region bounded by Eqs. (4) and (5) are a close fit to the modeled values, even though we had assumed the average refractive index of silicon oxide and target ssDNA in the

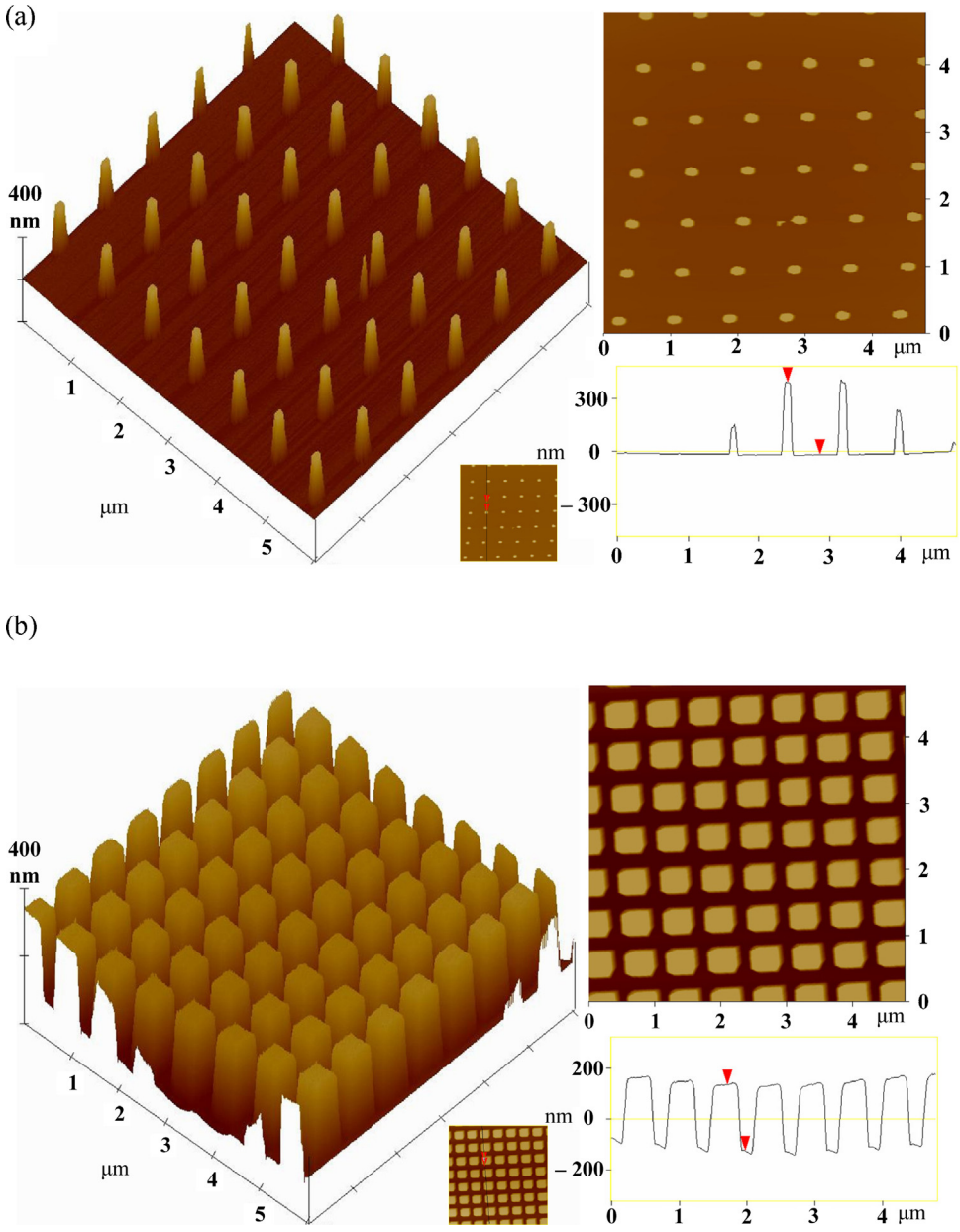

Fig. 3. AFM topographic images [3D (left), 2D (right), and line cross-sectional (right) analysis] of the oligonucleotides-modified NPLA (a) before and (b) after target ssDNA binding.

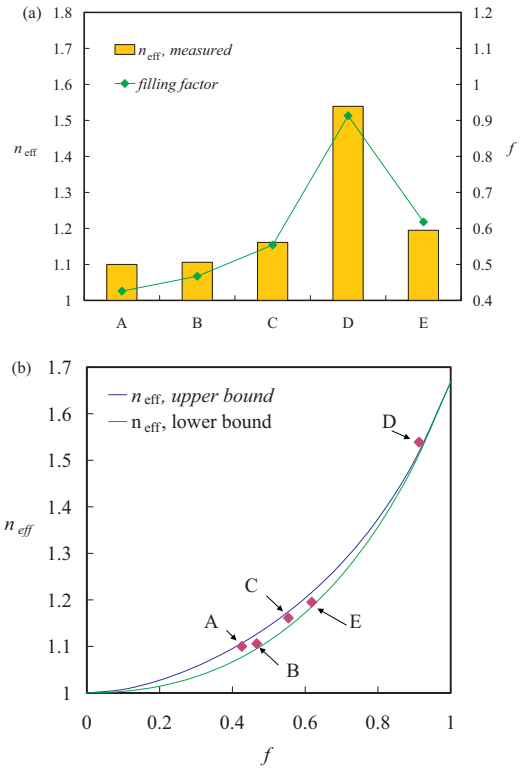

Fig. 4. (a) Values of n_{eff}, measured using ellipsometry, of (A) bare NPLA, (B) MPTES-NPLA, (C) oligonucleotides-modified NPLA, (D) oligonucleotides-modified NPLA after target ssDNA coupling, and (E) oligonucleotides-modified NPLA after binding the control ssDNA. (b) Values of n_{eff} of samples A–E plotted with respect to their values of f, fitted to Eqs. (4) and (5).

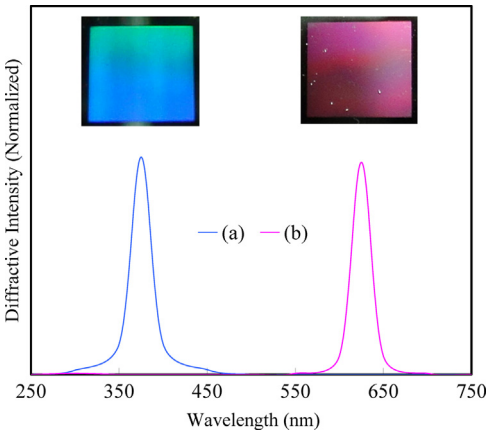

Fig. 5. (a) Diffraction spectra of the oligonucleotides-modified NPLA (a) before and (b) after target ssDNA hybridizing. *Insets*: Photographic images of samples (a) and (b), demonstrating the grating effect of the NPLA.

equations. Accordingly, the model perfectly matched the measured data when the geometrical parameters of the NPLA typically changed. The upward concave curves for the values of n_{eff} of the NPLA plotted with respect to the filling factors are consistent with previous reports [34,40].

The variation of the periodic structures can tune light propagation, which holds technological implications in various areas. Much progress has been made in the fabrication of ordered arrays that are responsive to external stimuli, which result in the modification of the lattice spacing of the opal structures [41]. Accordingly, the wavelength of diffraction of these ordered arrays shifts due to the change of photonic band gap (PBG). For diffraction-based applications, it is critical to engineer ordered arrays to exhibit bright and structure-based color. The oligonucleotides-NPLA films responded rapidly and sensitively to the target ssDNA, producing diffraction with high color purity. The diffraction could shift its peak position larger than 300 nm and retain full width at half maximum (FWHM) in the range of 150–200 nm. Fig. 5 presents diffraction spectra of oligonucleotides-modified NPLA and oligonucleotides-modified NPLA after target ssDNA hybridizing, peaking at 375, and 625 nm, respectively. The narrow FWHM suggests the preservation of the ordered structure of NPLA during the ssDNA hybridization [42]. The inset to Fig. 5 displays photographic images, obtained at angles β of approximately 15°, of the oligonucleotides-modified NPLA before and after hybridizing with target ssDNA (Fig. 1). We prepared the NPLA into a die using an etching process with a contact mask (1 cm × 1 cm). The light impinging the sample at an incident angle was linearly polarized, with the electric field vibration parallel (p) or perpendicular (s) to the plane of incidence; therefore, the reflected light was also p- or s-polarized. In this study, we observed the reflection of the NPLA through the naked eye under an invariable angle β [43]. The color of the oligonucleotides-modified NPLA was light blue prior to hybridizing with target ssDNA; it underwent an obvious color change to red after target ssDNA hybridizing. The ability to visualize such a color change provides the ability to rapidly and conveniently detect a specific ssDNA. The diffractive effect of a grating is dependent on its period and/or the angle of observation when its structural scale is larger than the wavelength of the incident light. Therefore, in this study we fixed both the period and angle of observation. These observed colors are closed to the peak positions of oligonucleotides-modified NPLA before and after hybridizing with target ssDNA.

We determined the sensitivity of the oligonucleotides-modified NPLA in a previous study [38]. Fig. 6a displays the relationship between the hybridizing concentration of target ssDNA and the n_{eff} in the duration (10 min). The variation in pillar scale within a period of 10 min occurred over the ssDNA concentration range 0.1–3.2 ng/μL, with the majority of the variation occurring between 0.2 and 0.4 ng/μL, defining the cut-off values. Thus, the quantity of target ssDNA that hybridized with the oligonucleotides-modified NPLA increased during that period upon treatment with 0.4 ng/μL of target ssDNA. In other words, the quantity of target ssDNA that hybridized onto the pillars might not be sufficient to generate a significant change in either the filling factor or the value of n_{eff} of the NPLA after 10 min if its concentration were less than 0.4 μg/mL. If the sample were immersed in below 0.4 ng/μL target ssDNA solution for a longer period of time (e.g., 30 min), then the value of n_{eff} would presumably change more significantly. Nevertheless, we expected the sample to respond to some degree within the 10-min period of the ssDNA detection. The n_{eff} increased slightly with increasing the concentration of control ssDNA, indicated that mismatch of ssDNA occurred. We generated this plot by measuring the values of n_{eff} of the oligonucleotides-modified samples to obtain a background reading for each ssDNA concentration. Fig. 6b shows four diffraction spectra collected from oligonucleotides-modified NPLA after hybridizing with various concentrations of target ssDNA in the duration. The red shift of diffraction spectra within a period of 10 min occurred apparently over the ssDNA concentration range 0.4–3.2 ng/μL. We observe approximately linear increases in peak position of the NPLA layer upon increasing concentration to 3.2 ng/μL. The peak position reached a plateau (650 nm), indicating the completely hybridizing of target ssDNA with the oligonucleotides moieties. During the red shift of the diffraction spectra from 400 nm (0.4 ng/μL) to 650 nm (3.2 ng/μL), the full width at half maximum (FWHM) stayed narrow with the estimation of ca. 50 nm. It is intriguing to understand the peak shift.

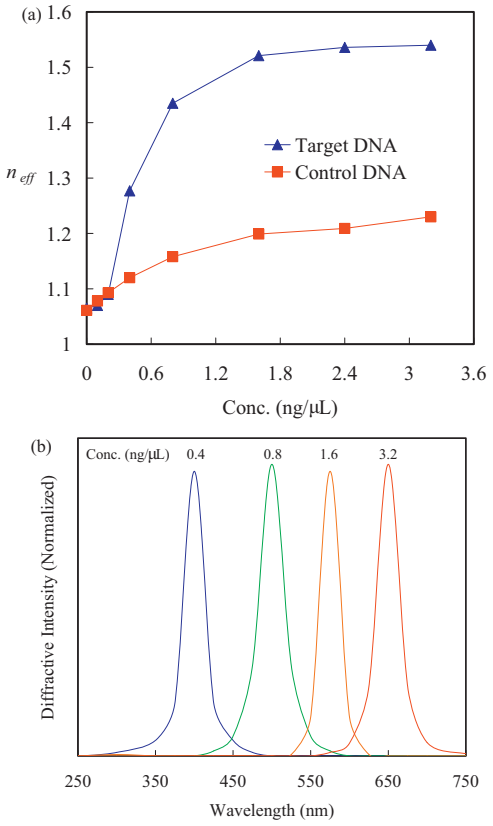

Fig. 6. Changes in the values of (a) n_{eff} of the NPLA plotted with respect to the concentration of target and control ssDNA after hybridizing for 10 min. (b) Diffraction spectra of the oligonucleotides-modified NPLA after hybridizing target ssDNA with 0.4, 0.8, 1.6 and 3.2 ng/μL concentrations for 10 min.

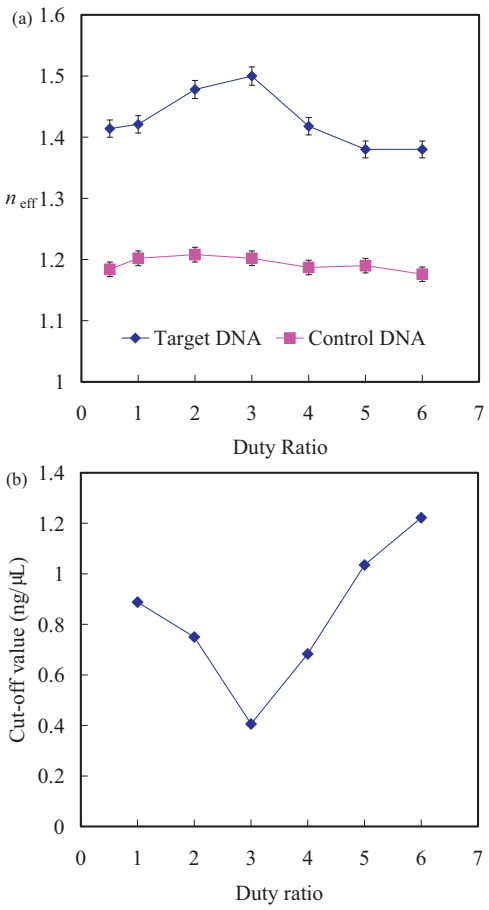

Fig. 7. (a) Values of n_{eff} of oligonucleotides-modified NPLA after binding the target ssDNA and control ssDNA, and (b) cut-off values of oligonucleotides-modified NPLA plotted with respect to the duty ratio of the NPLA.

The diffraction peak position (λ_{max}) of NPLAs was estimated by the following equation [44]:

$$k \cdot \lambda_{max} = \left(\frac{8}{3}\right)^{1/2} d \cdot n_{eff} \cdot \sin\theta \quad (6)$$

where k is the order of Bragg diffraction and θ is the glancing angle between the incident light and diffraction planes. In our study, k is a constant and θ is fixed at 75°. Thus, there are two factors affecting λ_{max}, d is the scale of pillars and n_{eff} is the average refractive index of NPLAs. When target ssDNA was hybridized with the oligonucleotides-modified NPLA, the red shift of λ_{max} was claimed to be a pure consequence of the increase of d, with the change of n_{eff} alone leading to 1–2 nm blue shift [45]. These results indicate that the inherent sensitivity and selectivity of ellipsometry-measured changes in refractive index across an interface as a result of ssDNA adsorption could be enhanced through the application of an NPLA structure.

Fig. 7a presents the values of n_{eff} of the NPLA plotted with respect to the duty ratios (i/w, Fig. 1), after the hybridizing of 0.4 ng/μL target ssDNA and the control ssDNA for 10 min. The values of n_{eff} increased with the duty ratio from 0.5 to 3, but decreased upon increasing duty ratio from 3 to 6. The largest change in the values of n_{eff} of the oligonucleotides-modified NPLA after hybridizing with target ssDNA occurred for duty ratio of NPLA at 3. When the spacing (i) scale of oligonucleotides-modified NPLA is smaller than that of target ssDNA, the NPLA layer may not permit the target ssDNA penetrate among the pillar spaces leading to obstruction of hybridization. As expected, the changes in the values of n_{eff} for the oligonucleotides-modified NPLA after hybridizing with target ssDNA decreased upon the duty ratio from 4 to 6. The results suggest that the sensitivity of the oligonucleotides-modified NPLA is determined on the proper scale of pillar spacing and target ssDNA. In addition, the changes in the values of n_{eff} for the oligonucleotides-modified NPLA after hybridizing with target ssDNA were much larger than those after coupling the control ssDNA. The results suggest that the oligonucleotides-modified NPLA specifically underwent an increase of filling volume after hybridizing with target ssDNA. Fig. 7b displays the relationship between the cut-off value (concentration) of target ssDNA, defined by a change in the value of n_{eff} of greater than 0.005, and the duty ratio. The cut-off values of target ssDNA decreased abruptly upon decreasing the duty ratio from 6 to 3, but increased thereafter. The lowest cut-off value of the oligonucleotides-modified NPLA after hybridizing with target ssDNA occurred for duty ratio of NPLA at 3, consistent with the results in Fig. 6a. These results suggest that a highly dense NPLA featuring immobilized oligonucleotides moieties might not possess sufficient space for complete binding of the target ssDNA. We generated this plot by measuring the values of n_{eff} of the oligonucleotides-modified samples to obtain a background reading for each ssDNA concentration. In addition, the change in color when the target ssDNA attached to the oligonucleotides-modified NPLA could be detected by the naked eye when the duty ratio was less than 5. In this present study, we prepared NPLAs that functioned as platforms for a selective ssDNA detection. The visual method of detection resulted from the target ssDNA being bound only to the oligonucleotides-modified regions. The change in color observed when illuminating the nanometer-scale grating arose most likely from the change in the effective refractive index during the coupling of the target ssDNA.

4. Conclusions

We substantially modified a specific oligonucleotides onto a pillar-structured surface over a large area, obtaining a system capable of ssDNA detection. By selecting a suitably functional oligonucleotides and optimizing the hybridizing of ssDNA, the scale of the nanostructures could be varied to maximize the responsiveness of the device. Although we could not exclude the effects of desorption of the target ssDNA after hybridizing with the oligonucleotides, the filling behavior of the target ssDNA among the pillars was sufficiently robust to survive the subsequent processing and yield a consistent, detectable signal for the effective refractive index. NPLAs are simple structures that allow the generation of hybridization surfaces without the need for any prior treatment or complicated processing. Because measurements of effective refractive index are not susceptible to small defects, any non-uniformities resulting from the fabrication process will not dramatically influence the results of the analyses. Although there are opportunities to improve the effects of SPR to generate optical biosensors, the current format described herein appears to be equally effective. Moreover, light reflected from the NPLA at an angle of 15° appeared pure blue and red to the naked eye before and after binding of the target ssDNA, respectively. This simple sensor might be able to detect other ssDNAs with apparent color changes, as well as any cells, with specific antigens, whose volume is sufficient to fill in the pillar structure when bound to the silicon surface.

Acknowledgments

We thank the National Science Council of the Republic of China for supporting this research financially and the National Nano Device Laboratory for assistance with the electron beam lithography and RIE.

References

[1] S. Weiss, Science 283 (1999) 1676.
[2] P. Zhang, T. Beck, W. Tan, Angew. Chem. Int. Ed. 40 (2) (2001) 402.
[3] X. Zhao, R. Tapec-Dytioco, W. Tan, J. Am. Chem. Soc. 125 (2003) 11474.
[4] R. Edgar, M. McKinstry, J. Hwang, A.B. Oppenheim, R.A. Fekete, G. Giulian, C. Merril, K. Nagashima, S. Adhya, Proc. Natl. Acad. Sci. U.S.A. 103 (13) (2006) 4841.
[5] M.A. Cooper, Anal. Bioanal. Chem. 377 (2003) 834.
[6] F. He, Y. Tang, M. Yu, F. Feng, L. An, H. Sun, S. Wang, Y. Li, D. Zhu, G.C. Bazan, J. Am. Chem. Soc. 128 (2006) 6764.
[7] J.-K. Chen, J.-H. Wang, C.-C. Cheng, J.-Y. Chang, ACS Appl. Mater. Interfaces 5 (2013) 2959–2966.
[8] J.B. Goh, P.L. Tam, R.W. Loo, M.C. Goh, Anal. Biochem. 313 (2003) 262–266.
[9] H.H. Jeong, N. Erdene, J.H. Park, D.H. Jeong, H.Y. Lee, S.K. Lee, Biosens. Bioelectron. 39 (2013) 346–351.
[10] J.-K. Chen, P.-C. Pai, J.-Y. Chang, S.-K. Fan, ACS Appl. Mater. Interfaces 4 (2012) 1935–1947.
[11] K.D. Mohan, A.L. Oldenburg, Opt. Express 20 (2012) 18887–18897.
[12] F.J. Sainz-Gonzalo, C. Elosua, J.F. Fernandez-Sanchez, C. Popovici, I. Fernandez, F.L. Ortiz, F.J. Arregui, I.R. Matias, A. Fernandez-Gutierrez, Sens. Actuators B 173 (2012) 254–261.
[13] H. Neubert, E.S. Jacoby, S.S. Bansal, R.K. Iles, D.A. Cowan, A.T. Kicman, Anal. Chem. 74 (2002) 3677–3683.
[14] W. Yeh, J. Kleingartner, A.C. Hillier, Anal. Chem. 82 (2010) 4988–4993.
[15] C.L. Chang, G. Acharya, C.A. Savran, Appl. Phys. Lett. 90 (2007) 233901.
[16] G. Acharya, C.L. Chang, D.D. Doorneweerd, E. Vlashi, W.A. Henne, L.C. Hartmann, P.S. Low, C.A. Savran, J. Am. Chem. Soc. 129 (2007) 15824–15829.
[17] J.K. Chen, B.J. Bai, J. Phys. Chem. C 115 (2011) 21341–21350.
[18] J.-K. Chen, G.-Y. Zhou, C.-F. Huang, J.-Y. Chang, ACS Appl. Mater. Interfaces 5 (2013) 3348–3355.
[19] C. Ma, Y. Jiang, X. Yang, C. Wang, H. Li, F. Dong, B. Yang, K. Yu, Q. Lin, ACS Appl. Mater. Interfaces 5 (6) (2013) 1990–1996.
[20] M. Hirade, H. Nakanotani, M. Yahiro, C. Adachi, ACS Appl. Mater. Interfaces 3 (2011) 80–83.
[21] J. Chen, J. Wang, C. Cheng, J. Chang, F. Chang, Appl. Phys. Lett. 102 (2013) 151906.
[22] Y.G. Wang, S.W. Chang, C.C. Chen, C.H. Chiu, M.Y. Kuo, M.H. Shih, H.C. Kuo, Appl. Phys. Lett. 99 (2011) 251111.
[23] C. Somaschini, S. Bietti, N. Koguchi, S. Sanguinetti, Nano Lett. 9 (2009) 3419–3424.
[24] Z.Q. Sun, Y. Li, J.H. Zhang, Y.F. Li, Z.H. Zhao, K. Zhang, G. Zhang, J.R. Guo, B. Yang, Adv. Funct. Mater. 18 (2008) 4036–4042.
[25] R. Near, C. Tabor, J.S. Duan, R. Pachter, M. El-Sayed, Nano Lett. 12 (2012) 2158–2164.
[26] G. Ye, X. Wang, Biosens. Bioelectron. 26 (2010) 772–777.
[27] H.L. Huang, J.-K. Chen, M.P. Houng, Sens. Actuators B 177 (2013) 833–840.
[28] A. Sato, S. Konishi, H. Tamura, H.G. Stickland, H.M. Whitney, A.G. Smith, H. Matsumura, T. Inoue, Biochemistry 49 (30) (2010) 6400–6410.
[29] J.K. Chen, C.Y. Hsieh, C.F. Huang, P.M. Li, S.W. Kuo, F.C. Chang, Macromolecules 41 (2008) 8729–8736.
[30] J.K. Chen, A.-L. Zhuang, J. Phys. Chem. C 114 (2010) 11801–11809.
[31] W.C.E. Schofield, J. McGettrick, T.J. Bradley, J.P.S. Badyal, S. Przyborski, J. Am. Chem. Soc. 128 (2006) 2280–2285.
[32] J. Habicht, M. Schmidt, J. Rühe, D. Johannsmann, Langmuir 15 (1999) 2460–2465.
[33] E.B. Grann, M.G. Moharam, D.A. Pommet, J. Opt. Soc. Am. A 11 (1994) 2695.
[34] F.T. Chen, H.G. Craighead, Opt. Lett. 20 (1995) 121–123.
[35] J.L. Jackson, S.R. Coriell, J. Appl. Phys. 39 (1968) 2349.
[36] V. Artel, R. Cohen, I. Aped, M. Ronen, D. Gerber, C.N. Sukenik, Langmuir 29 (2013) 191–198.
[37] X. Wang, M. Lieberman, Langmuir 19 (2003) 7346–7353.
[38] J. Chen, G. Zhou, C. Chang, Sens. Actuators B 186 (2013) 802–810.
[39] S. Niu, G. Singh, R.F. Saraf, Biosens. Bioelectron. 23 (2007) 714–720.
[40] H. Kikuta, H. Toyota, W. Yui, Opt. Rev. 10 (2003) 63–73.
[41] J. Chen, G. Zhou, C. Huang, F. Ko, Appl. Phys. Lett. 102 (2013) 251903.
[42] T. Hellweg, Angew. Chem. Int. Ed. 48 (2009) 6777–6778.
[43] J.-K. Chen, G.-Y. Zhou, C.-J. Chang, A.-W. Lee, F.-C. Chang, Biosens. Bioelectron. 54 (2014) 35–41.
[44] M.M.W. Muscatello, L.E. Stunja, S.A. Asher, Anal. Chem. 81 (2009) 4978–4986.
[45] J.Y. Wang, Y. Cao, Y. Feng, F. Yin, J.P. Gao, Adv. Mater. 19 (2007) 3865–3871.

Biographies

Jem-Kun Chen received his BS (1996) and MS (1998) in Chemical Engineering from National Tsing Hua University (Taiwan) and his PhD (2003) in Applied Chemistry from National Chiao Tung University (Taiwan). From 2003 to 2004, he was a postdoctoral fellow with Professor Samukawa in the Department of Fluid Science at Touhoku University, Sendai (Japan), where he investigated the fabrication and analysis of quantum dots and nanodisks. In 2005, he joined the Department of Biomechatronics Engineering at Ping-tung University (Taiwan) as an assistant professor. Since 2006, he has been an assistant professor of Polymer Engineering at National Taiwan University of Science and Technology. He is an associate professor of Materials Science and Engineering at National Taiwan University of Science and Technology from 2009 to 2012. He is promoted as a professor of Materials Science and Engineering at National Taiwan University of Science and Technology from 2013 to now. His current research emphasizes the processing, characterization, modeling, and optimization of polymer brush devices for optical and biological sensors. He has published over 60 articles (2004–2013).

Gang-Yan Zhou received his MS (2008) from the Department of Materials Science and Engineering of National Taiwan University of Science and Technology, from research conducted in Dr. Chen's laboratories. His research interests are centered mainly on the development of semiconductor technology. He currently works for Taiwan Power Company as a process engineer.

Chi-Jung Chang received his PhD (2004) from the Department of Material Science and Engineering of National Chiao Tung University (Taiwan). From 2004 to 2008, he was a researcher at the Industrial Technology Research Institute (ITRI) of Taiwan, where he investigated the composition of photocurable pigment-type inkjet inks. In 2009, he joined the Department of Chemical Engineering of Feng Chia University (Taiwan) as a professor. His current research emphasizes nanoparticles and hydrophobic surfaces; he has published over 40 articles (2004–2012).

Chih-Chia Cheng received his PhD degree (2008) from the Department of Applied Chemistry, National Chiao-Tung University, Taiwan. From 2008 to now, he is a postdoctoral in Department of Applied Chemistry, National Chiao-Tung University, where he worked on the research about the synthesis of the self-assembled macromolecule. He has published over 20 articles (2008–2013).